RESEARCH ON THE ENERGY EFFICIENCY IMPROVEMENT OF CLOSED LOOP WASTEWATER SOURCE HEAT PUMP WITH DIRECT-EXPANSION HEAT EXCHANGER

Yuanyuan Liu[1], Tianxiang Jia[1], Jing Wang[2], Yang Li*[2], Jun Zhao[2], Yaze Wang[2], Xinlei Liang[1]

[1]Huadian Zhengzhou Mechanical Design Institute Company Limited, Zhengzhou 450046, China

[2]School of Mechanical Engineering, Tianjin University, Tianjin 300350, China

[*] Corresponding author; E-mail: liyangtju@tju.edu.cn

The closed-loop wastewater source heat exchanger (WSHE) has advantages such as being non-clogging and resistant to corrosion, but their heat transfer efficiency is relatively low, therefore it is still not the mainstream form of heat exchanger of wastewater source heat pump (WSHP). A novel CO_2 direct-expansion wastewater source heat exchanger (DX-WSHE) is proposed in this paper, aiming to significantly improve the heat transfer rate of the heat exchanger and the energy efficiency of the heat pump system. The direct-expansion heat transfer process is complex, large grid number and long calculation time will be required if calculated by conventional numerical simulation software. Therefore, a three-dimensional transient heat transfer model was developed based on the thermal resistance and capacity model, which offers the advantages of fast computation speed and strong flexibility. The heat transfer and energy efficiency characteristics under different parameters were studied. The coefficient of performance (COP) of the direct-expansion wastewater source heat pump (DX-WSHP) can be increased by 31.0% compared to conventional design, and the heat flux of the direct-expansion wastewater source heat exchanger can be up to 250 W/m for the standard group. Compared with conventional designs, the direct-expansion wastewater source heat pump has excellent heat transfer and energy efficiency capabilities, which is a promising building energy saving and emission reduction technology.

Key words*: wastewater source heat pump, direct-expansion heat exchanger, thermal resistance and capacity model, numerical simulation*

1. Introduction

The extensive utilization of traditional energy sources leads to the increase of CO_2 emission [1]. At present, building energy consumption accounts for about 30% of the total energy consumption, about 65% of household energy consumption is used for building air conditioning, heating and household heating **Error! Reference source not found.**. It can be seen that reducing building energy consumption is helpful to reduce global carbon emissions and achieve energy conservation and emission reduction. Among low-grade energy sources, urban sewage is one of the clean energy sources that can be recycled [3]. Using wastewater source heat pump (WSHP) for building heating and

cooling is an effective means to reduce building energy consumption and CO_2 emissions [4]. Conventional WSHP can be divided into two categories: direct and indirect systems. As shown in Fig. 1, it is an efficient, environmentally friendly and energy-saving heat pump technology with comprehensive functions and stable operation.

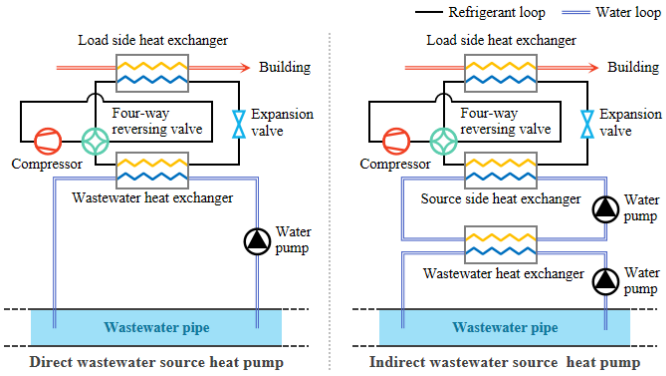

Fig.1 System diagram of direct and indirect wastewater source heat pump

In order to compare the advantages of WSHP in energy saving, many scholars have carried out research and verification. Du et al. [5] made a comprehensive comparison between traditional heating and cooling systems and various heat pump systems by means of technical and economic analysis and life cycle assessment, and proved that WSHP has the lowest greenhouse gas emission and the lowest production cost. Ozcan et al. [6] simulated and evaluated the performance of WSHP for district heating through a series of engineering equation solvers based on 20 different cases, which proved its advantages in sustainability. At the same time, some scholars focus on how to improve the operational efficiency of WSHP and study the factors that affect its operational efficiency. Wang et al. [7] made an experimental analysis on a new type of nonmetallic immersed WSHE with rare earth elements, which proved that its heat exchange capacity was much higher than that of the traditional heat exchanger. Zhang et al. [8] applied falling film evaporator to WSHP to improve the total heat transfer coefficient of evaporator and the performance of heat pump.

Regardless of whether it is a direct or indirect WSHP, the wastewater needs to enter one of the heat exchangers, which may lead to issues such as clogging and corrosion, and the intermediate heat exchange process will to some extent reduce the heat transfer efficiency. Furthermore, for cooling applications, the system energy efficiency will be reduced due to the higher temperature of the wastewater. In order to solve the above problems, this paper proposes a direct expansion WSHP (DX-WSHP). In DX-WSHP, no water loop is needed, and the refrigerant is directly circulated through the closed-loop direct expansion sewage source heat exchanger (DX-WSHE) in the sewage pipeline. Although the application and research of direct expansion WSHP is still limited, due to the further exploration of geothermal resources [9], the technology of ground source heat pump has made great progress [10], among which there have been some researches on direct expansion ground source heat pump (DX-GSHP). Because sewage pipes are buried in soil, DX-WSHP can also be considered as a broader category based on DX-GSHP. At present, there have been some researches on DX-GSHP.

Gao et al. [11] established the whole system model of direct expansion heat pump, and explored the influence of key parameters on heat exchange and COP. Nguyen et al. [12] established the thermal resistance and heat capacity model of direct expansion heat pump, and studied the effects of different inlet pressures and mass flow rates. Ahsaee and Ameri also conducted a series of theoretical

researches on the CO_2 DX-WSHP with horizontal DX-GHE, a base model was proposed in [13], an expander and an internal heat exchanger were added in [14], and an exergo-economic analysis was conducted in [15]. However, the above-mentioned studies all utilized one-dimensional steady-state heat transfer models, which may deviate from the actual heat transfer process and make it difficult to calculate under dynamic operating conditions.

At present, there are few studies on the combination of direct expansion heat pump and WSHP. Therefore, a DX-WSHE three-dimensional transient heat transfer model based on thermal resistance and heat capacity model (TRCM) is established in this paper. The model was then used to study the heat transfer characteristics under various parameter influences. Subsequently, a system model was developed to calculate the system's energy efficiency under different operating conditions. To facilitate comparison with other studies, CO_2, which is known for its environmental friendliness and good heat transfer performance, is also used as the refrigerant in this study.

2. Models

2.1. Physical model

Fig. 2 is the system diagram of DX-WSHP.

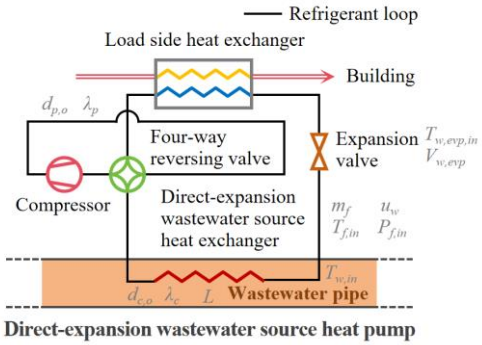

Fig.2 System diagram of direct-expansion wastewater source heat pump

The DX-WSHP has the following advantages:

(1) High heat transfer efficiency: with the refrigerant directly circulating through the wastewater for heat exchange, the heat pump can efficiently extract or release heat, resulting in improved heat transfer efficiency.

(2) Lower energy consumption: the absence of water-side circulation pumps reduces the total power consumption, resulting in an improved coefficient of performance (COP) for the system.

(3) Simplified system structure: by not requiring the extraction of wastewater, the DX-WSHP avoids issues like heat exchanger clogging, and reducing system complexity and maintenance costs.

(4) Suitable for cooling applications: in cooling mode, the DX-WSHE serves as a condenser or gas cooler (supercritical condition). The temperature difference between the refrigerant and the wastewater is significantly higher than that in conventional systems, ensuring higher energy efficiency.

2.2. DX-WSHE model

The direct-expansion heat transfer process is complex, large grid number and long calculation time will be required if calculated by conventional numerical simulation software. Therefore, a three-dimensional transient heat transfer model was developed based on the TRCM, which offers the advantages of fast computation speed and strong flexibility.

The TRCM of the DX-WSHE is based on the following assumptions:

(1) The properties of the CO_2 pipe, wastewater, wastewater pipe, and soil are homogeneous and constant, whereas the properties of CO_2 are determined by temperature and pressure and were accessed through the NIST REFPROP [16].

(2) In addition to the inlet and outlet of CO_2 and wastewater, the external boundaries of the model are considered adiabatic.

The model consists of five regions, namely CO_2, CO_2 pipe, wastewater, wastewater pipe, and soil, denoted by subscripts *f*, *p*, *w*, *c*, and *s*, respectively. Each region is divided into several control volumes. For the soil region, due to the more significant temperature changes closer to the wastewater pipe, the control volumes of the soil region in the positive/negative *x*-axis and negative *y*-axis directions was densified. The densification was carried out in a geometric progression with a common ratio of 1.1. As for the soil in the positive *y*-axis direction, it was divided at equal intervals since it is shallower in depth. The control volumes segmentation is shown in Fig. 3. The total number of control volumes in the baseline model is 3090.

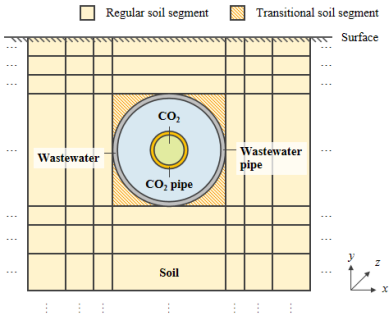

Fig.3 Control volumes segmentation of DX-WSHE

Fig. 4 is a schematic diagram of the TRCM network for the heat transfer model. Taking the *i*-th layer and the (*i*+1)-th layer as an example, the diagram shows the following elements: blue solid circles represent temperature nodes with thermal capacity; yellow hollow circles represent temperature nodes without thermal capacity, usually at the interfaces between two regions; red zigzag lines represent regular thermal resistances; green zigzag lines with arrows represent equivalent thermal resistance, which are used to characterize CO_2 and wastewater flow.

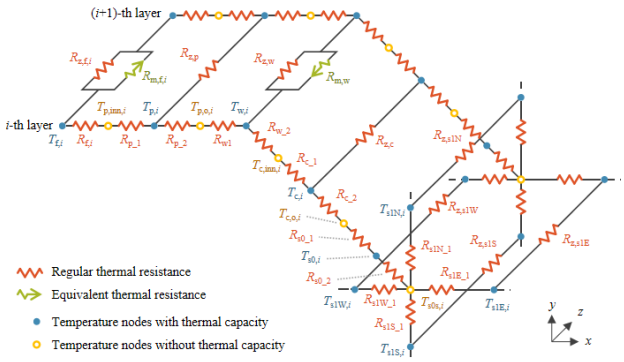

Fig.4 Network of thermal resistance and capacity model

The thermal resistance of the convective heat transfer process of CO_2 is calculated as follows:

$$R_{\mathrm{f}} = \frac{1}{\mathrm{Nu}_{\mathrm{f}} \lambda_{\mathrm{f}} \pi} \tag{1}$$

$$\mathrm{Nu}_{\mathrm{f}} = 0.01 \mathrm{Re}_{\mathrm{f}}^{0.89} \mathrm{Pr}_{\mathrm{f}}^{-0.14} \left(\frac{\rho_{\mathrm{f,Wall}}}{\rho_{\mathrm{f}}} \right)^{0.93} \left(\frac{\lambda_{\mathrm{f,Wall}}}{\lambda_{\mathrm{f}}} \right)^{0.22} \left(\frac{\mu_{\mathrm{f,Wall}}}{\mu_{\mathrm{f}}} \right)^{-1.13} \tag{2}$$

The thermal resistance of heat conduction in the *xy* direction of the CO_2 pipe is calculated as follows:

$$R_{\mathrm{p\_1}} = R_{\mathrm{p\_2}} = \frac{\ln\left(d_{\mathrm{p,o}} / d_{\mathrm{p,inn}}\right)}{4\pi\lambda_{\mathrm{p}}} \tag{3}$$

The thermal resistance of the convective heat transfer process in wastewater is calculated as follows:

$$R_{\mathrm{w\_1}} = R_{\mathrm{w\_2}} = \frac{1}{2h_{\mathrm{w}}\pi d_{\mathrm{p,o}}} \tag{4}$$

$$h_{\mathrm{w}} = \frac{\mathrm{Nu}_{\mathrm{w}} \lambda_{\mathrm{w}}}{d_{\mathrm{hyd,w}}} \tag{5}$$

$$\mathrm{Nu}_{\mathrm{w}} = \left(f_{\mathrm{w}}/8\right)\left(\mathrm{Re}_{\mathrm{w}} - 1000\right)\mathrm{Pr}_{\mathrm{w}} \Big/ \left(1 + 12.7\left(f_{\mathrm{w}}/8\right)^{1/2}\left(\mathrm{Pr}_{\mathrm{w}}^{2/3} - 1\right)\right) \tag{6}$$

$$f_{\mathrm{w}} = \left(0.79\,\mathrm{Re}_{\mathrm{w}} - 1.64\right)^{-2} \tag{7}$$

The equation for the equivalent thermal resistance that represents the CO_2 flow is as follows:

$$R_{\mathrm{m,f}} = \frac{\Delta z}{\overline{m_{\mathrm{f}}}\, c_{\mathrm{f}}} \tag{8}$$

The equation for the equivalent thermal resistance that represents the wastewater flow is similar to that of CO_2. The calculation method for the thermal resistance of heat conduction in the *xy* direction of the wastewater pipe is the same as that for the CO_2 pipe. The thermal resistance of the regular soil segments are calculated based on Fourier's law. The above equations are omitted.

To address the heat transfer between circular (wastewater pipe) and square (soil) control volumes, a thermal resistance equation for the transitional soil segment (subscript s0) was established based on the shape factor method, as shown below:

$$R=\frac{\ln\left(\left(\int_0^1\left(1+w^N\right)^{-2/N}\mathrm{d}w\right)^{-1}\right)}{2\pi\lambda}\quad N\geq 3 \tag{9}$$

The equation represents the general thermal resistance expression for shapes such as a regular *N*-sided polygon with the inner inscribed circle subtracted. The thermal resistance calculation equation for the heat conduction in the *z*-direction of each control volume is as follows:

$$R_{\mathrm{z}}=\frac{\left(\Delta z\right)^2}{\bar{\lambda}A} \tag{10}$$

For each control volume *A*, assuming the number of control volumes that are connected to *A* is *B*, then the heat transfer equation can be expressed as:

$$C_{\mathrm{A}}\frac{\mathrm{d}T_{\mathrm{A}}}{\mathrm{d}\tau}=\sum_{b=1}^{B}\frac{T_b-T_{\mathrm{A}}}{R_{\mathrm{A\_}b}} \tag{11}$$

$$\begin{bmatrix}\frac{\mathrm{d}T_1}{\mathrm{d}\tau}\\ \frac{\mathrm{d}T_2}{\mathrm{d}\tau}\\ \vdots\\ \frac{\mathrm{d}T_n}{\mathrm{d}\tau}\end{bmatrix}=\begin{bmatrix}f\left(C_1,R_{1\_2},\cdots R_{1\_n}\right) & f\left(C_1,R_{1\_2}\right) & \cdots & f\left(C_1,R_{1\_n}\right)\\ f\left(C_2,R_{2\_1}\right) & f\left(C_2,R_{2\_1},\cdots R_{2\_n}\right) & & \vdots\\ \vdots & & \ddots & f\left(C_{n-1},R_{n-1\_n}\right)\\ f\left(C_n,R_{n\_1}\right) & \cdots & f\left(C_n,R_{n\_n-1}\right) & f\left(C_n,R_{n\_1},\cdots R_{n\_n-1}\right)\end{bmatrix}\begin{bmatrix}T_1\\ T_2\\ \vdots\\ T_n\end{bmatrix} \tag{12}$$

2.3. Node independent test

The way the nodes are divided can affect the calculation accuracy and the computational time. To reduce the computational time while maintaining calculation accuracy, a node independence test was conducted for the established TRCM. Since the heat transfer process mainly occurs inside the wastewater and CO_2, and the influence of the soil on the heat transfer is relatively small, the independence test focused on changing the layer-to-layer distance in the *z*-direction (d_z). A baseline case was created with d_z=0.5 m, and three control groups were set with d_z values of 1 m, 2 m, and 3.75 m. Comparative calculations were performed, and the results are shown in Fig. 5.

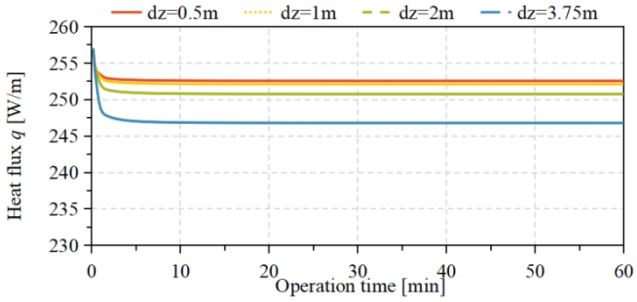

Fig.5 Node independent test result

The result indicates that the difference in heat transfer diminishes gradually, and when d_z=1 m, the heat transfer is almost consistent with d_z=0.5 m. The mean absolute percentage errors of heat flux *q* for d_z values of 1 m, 2 m, and 3.75 m compared to d_z=0.5 m are 0.17%, 0.70%, and 2.24%, respectively. Considering both the computational speed and the required calculation accuracy, d_z=1 m is selected as the actual value used in the model.

2.4. Heat pump system model

The system model of DX-WSHP is established based on the TRCM and integrating key components such as the compressor and the load-side heat exchanger.

Based on the manufacturer's sample data for the Dorin TCS340/4-D type compressor, fitting models for the volumetric efficiency η_{vol} and overall efficiency η_{tot} of the compressor were established. The sample data consists of 34 operating points, and various parameters such as enthalpy-entropy values and mass flow rate were calculated using theoretical thermodynamic cycle. Subsequently, the η_{vol} and η_{tot} were derived from these calculated parameters. Based on the modeling approach in relevant CO_2 heat pump studies [17], the fitting models for η_{vol} and η_{tot} are formulated with the compression ratio as the variable. The models are as follows:

$$\eta_{vol}=\begin{cases}\dfrac{0.66222\left(\dfrac{P_{com,out}}{P_{com,in}}\right)^2-2.532\left(\dfrac{P_{com,out}}{P_{com,in}}\right)+9.78408}{\left(\dfrac{P_{com,out}}{P_{com,in}}\right)^2-2.054\left(\dfrac{P_{com,out}}{P_{com,in}}\right)+9.06} & \dfrac{P_{com,out}}{P_{com,in}}\le 4.5283\\ \dfrac{0.39167\left(\dfrac{P_{com,out}}{P_{com,in}}\right)-1.6327}{\left(\dfrac{P_{com,out}}{P_{com,in}}\right)-4.2852} & \dfrac{P_{com,out}}{P_{com,in}}>4.5283\end{cases} \tag{13}$$

$$\eta_{tot}=\begin{cases}\dfrac{0.7432\left(\dfrac{P_{com,out}}{P_{com,in}}\right)^2-6.4657\left(\dfrac{P_{com,out}}{P_{com,in}}\right)+17.3231}{\left(\dfrac{P_{com,out}}{P_{com,in}}\right)^2-8.6279\left(\dfrac{P_{com,out}}{P_{com,in}}\right)+24.3694} & \dfrac{P_{com,out}}{P_{com,in}}\le 4.5283\\ \dfrac{0.43153\left(\dfrac{P_{com,out}}{P_{com,in}}\right)-1.8111}{\left(\dfrac{P_{com,out}}{P_{com,in}}\right)-4.2754} & \dfrac{P_{com,out}}{P_{com,in}}>4.5283\end{cases} \tag{14}$$

To facilitate modeling and analysis, the load-side heat exchanger is assumed to be a shell-tube heat exchanger. The load-side heat exchanger serves as the evaporator, which consists of two regions: phase change region and superheat region. The heat exchanger is divided into several small segments, and the energy conservation equation for each segment can be expressed as follows:

$$\begin{aligned}Q_{evp} &= m_f\left(H_{f,evp,out}-H_{f,evp,in}\right)\\ &= UA\frac{\left(T_{w,evp,in}-T_{f,evp,out}\right)-\left(T_{w,evp,out}-T_{f,evp,in}\right)}{\ln\left[\left(T_{w,evp,in}-T_{f,evp,out}\right)/\left(T_{w,evp,out}-T_{f,evp,in}\right)\right]}\\ UA &= \frac{\Delta L}{\left(R_{f,evp}+R_p+R_{w,evp}\right)}\\ &= \Delta L\left(\frac{1}{h_{f,evp}\pi d_{p,inn}}+\frac{\ln\left(d_{p,o}/d_{p,inn}\right)}{2\pi\lambda_p}+\frac{1}{h_{w,evp}\pi d_2}\right)^{-1}\end{aligned} \tag{15}$$

3. Results and discussions

3.1. Parametric analysis of DX-WSHE

To study the influence of various operating conditions, geometric design parameters, and physical properties on the heat transfer characteristics of the DX-WSHE, 10 different parameters were selected for comparative calculations. The parameters for the standard group and control group are shown in Table 1.

Table 1 Standard group and control group for the parametric analysis of DX-WSHE

Parameter	Unit	Standard group	Control group*
CO_2 mass flow rate m_f	kg/s	30	10~170, interval 20
Wastewater flow velocity u_w	m/s	0.1	0.05, 0.075, 0.2, 0.3, 0.5, 0.8
CO_2 inlet temperature $T_{f,in}$	℃	100	80~120, interval 5
Wastewater inlet temperature $T_{w,in}$	℃	23	19~27, interval 1
CO_2 inlet pressure $P_{f,in}$	MPa	10	7.5~12, interval 0.5
DX-WSHE length L	m	30	10~50, interval 5
CO_2 pipe outer diameter $d_{p,o}$	mm	12	8~16, interval 1
Wastewater pipe outer diameter $d_{c,o}$	mm	75	32, 40, 50, 110, 160, 200
CO_2 pipe thermal conductivity λ_p	W/(m·K)	398	0.1, 1, 10, 100
Wastewater pipe thermal conductivity λ_c	W/(m·K)	0.15	0.1, 1, 10, 100

* Note: if the standard group values are included, they will be automatically deleted.

Based on the results in Fig. 5, it can be observed that the flow of wastewater could effectively carry away the heat released by CO_2. Therefore, a steady state was reached after approximately 10 minutes of operation. Consequently, the operation time for the parametric analysis was set to 10 minutes for all cases.

Firstly, an analysis of the calculation results for the standard group was conducted. Fig. 6 (a) shows the temperature variation curves of CO_2, CO_2 pipe, and wastewater along the path. It can be observed that the most significant heat transfer occurs within the first 5 m, with CO_2 temperature rapidly decreasing.

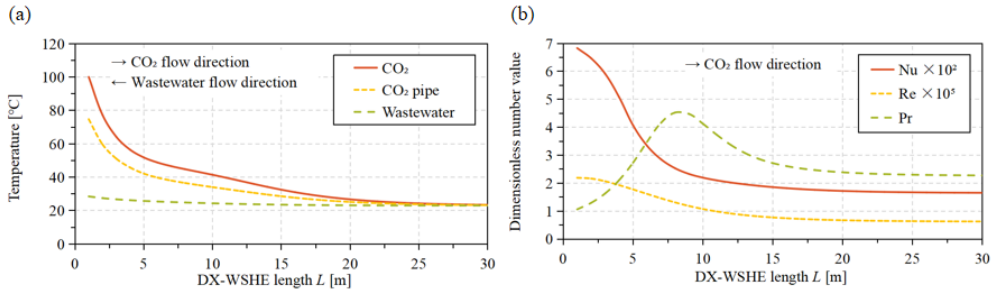

Fig.6 (a) Temperature variation along the path: standard group; (b) dimensionless number variation along the path

In addition, the dimensionless numbers *Nu*, *Re*, and *Pr* along the path are plotted in Fig.6 (b). It can be observed that the *Re* shows a decreasing trend initially followed by leveling off, while the *Pr* exhibits an increasing trend initially followed by a decrease. According to Eq. (3), the *Nu* is positively correlated with the *Re* and negatively correlated with the *Pr*. Therefore, the decrease in *Re* and increase in *Pr* within the first 5 m lead to a decrease in *Nu*. Subsequently, with the decrease in *Pr*, the variation of *Nu* becomes more gradual.

3.1.1 Influence of CO_2 mass rate and wastewater velocity

Fig. 7 (a) shows the variation of q and pressure drop ΔP with respect to m_f. As the m_f increases, the q shows synchronous growth, but the rate of increase gradually decreases. Meanwhile, the ΔP also

shows synchronous growth, and the rate of increase gradually rises. Therefore, when the m_f becomes too large, the improvement in heat transfer becomes less significant, but the ΔP and compressor power consumption will significantly increase. Hence, it is essential to choose an appropriate value for the m_f to balance heat transfer efficiency and operation cost.

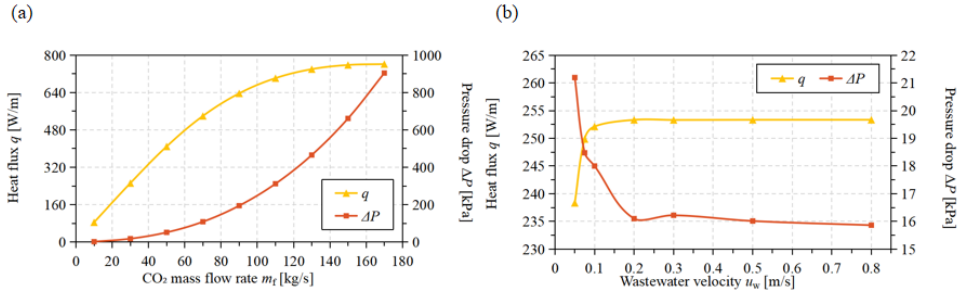

Fig.7 (a) Influence of CO_2 mass rate; (b) influence of wastewater velocity

Fig. 7 (b) shows the variation of q and ΔP with respect to u_w. When the u_w increases to 0.2 m/s, both the q and ΔP have reached a stable state, and thereafter, they show very little change as the u_w increases further.

3.1.2 Influence of inlet temperature of CO_2 and wastewater

Fig. 8 (a) shows the variation of q and ΔP with respect to $T_{f,in}$. As the $T_{f,in}$ increases, both the heat transfer rate and the pressure drop show a linear increase.

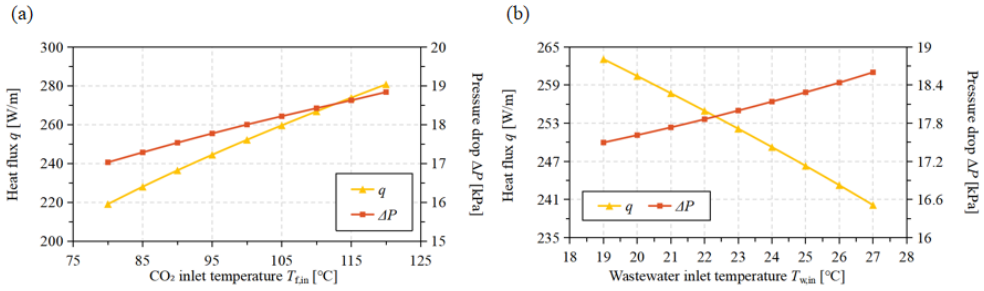

Fig.8 (a) Influence of CO_2 inlet temperature; (b) influence of wastewater inlet temperature

Fig. 8 (b) shows the variation of q and ΔP with respect to $T_{w,in}$. As the $T_{w,in}$ increases, the q shows a linear decreasing trend. Meanwhile, the ΔP exhibits a linear increasing trend, but its overall variation is relatively small compared to the influence of $T_{f,in}$.

3.1.3 Influence of CO_2 inlet pressure and DX-WSHE length

Fig. 9 (a) shows the variation of q and ΔP with respect to $P_{f,in}$. As the $P_{f,in}$ increases, the q initially shows an increasing trend and then decreases. This trend is likely due to the fact that at low pressures, the CO_2 is approaching its critical pressure, leading to significant changes in its properties. This may cause deterioration in heat transfer performance, and similar phenomena have been reported in previous studies of DX-GHE [18]. On the other hand, the ΔP decreases gradually as the $P_{f,in}$ decreases.

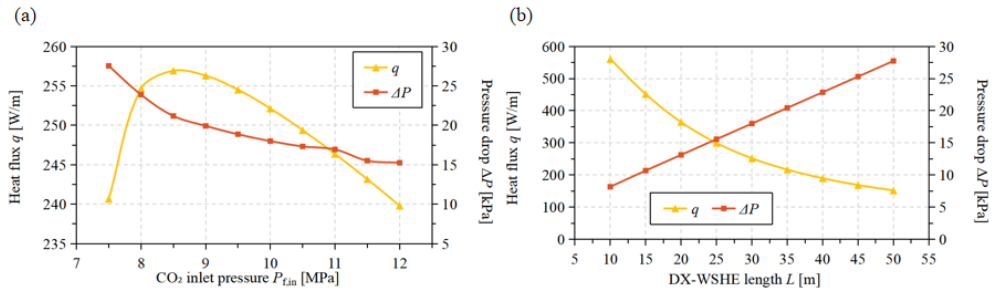

Fig.9 (a) Influence of CO_2 inlet pressure; (b) influence of DX-WSHE length

Fig. 9 (b) shows the variation of q and ΔP with respect to L. As the L increases, the q shows a gradually decreasing trend with a decreasing rate of reduction. On the other hand, the ΔP exhibits a roughly linear increasing trend with the increase in L.

3.1.4 Influence of outer diameter of CO_2 pipe and wastewater pipe

Please note that the thickness of the two types of pipes is not constant but calculated based on the principle of equal pressure endurance capacity. Fig. 10 (a) shows the variation of q and ΔP with respect to $d_{p,o}$. As the $d_{p,o}$ increases, the q shows a gradually increasing trend and tends to stabilize, but the actual variation is very small. Meanwhile, the ΔP exhibits a significant decreasing trend.

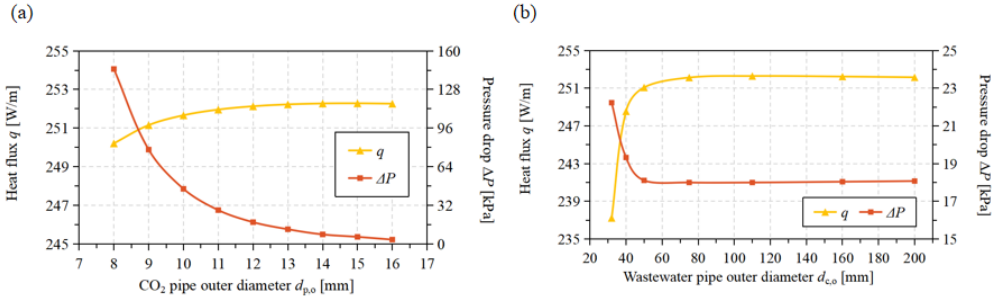

Fig.10 (a) Influence of CO_2 pipe outer diameter; (b) influence of wastewater pipe outer diameter

Fig. 10 (b) shows the variation of q and ΔP with respect to $d_{c,o}$. When the $d_{c,o}$ is less than 50 mm, reducing the $d_{c,o}$ will significantly decrease the q and increase the ΔP. In other words, when the $d_{c,o}$ is relatively large, it may be beneficial to consider adding more CO_2 pipes within the wastewater pipe to increase the total q.

3.1.5 Influence of thermal conductivity of CO_2 pipe and wastewater pipe

The λ_p of 398 W/(m·K) in the standard group is based on the properties of copper. Fig. 11 (a) shows the variation of q and ΔP with respect to λ_p. When the λ_p is lower than 10 W/(m·K), the q and ΔP will decrease/increase significantly with the decrease of λ_p. However, the material that can be used to make direct-expansion heat exchangers is usually metal, and the thermal conductivity is usually greater than 10 W/(m·K). Therefore, different CO_2 pipe materials have little influence on the heat transfer of DX-WSHE.

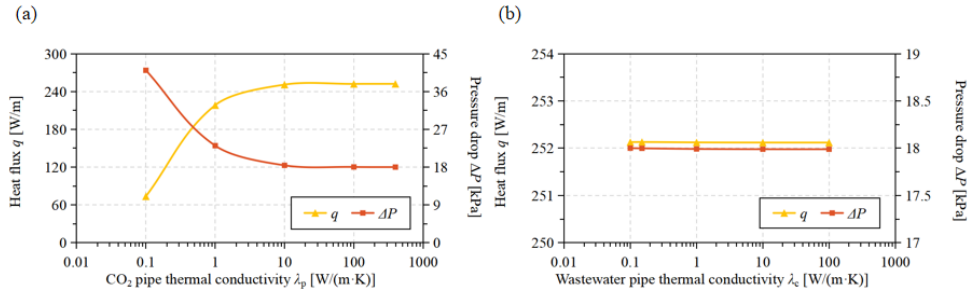

Fig.11 (a) Influence of thermal conductivity of CO_2 pipe; (b) influence of thermal conductivity of wastewater pipe

The λ_c of 0.15 W/(m·K) in the standard group is based on the properties of PVC. Fig. 11 (b) shows the variation of q and ΔP with respect to λ_c. The q and ΔP show little variation with changes in the λ_c.

3.2. Parametric analysis of DX-WSHP

Based on the DX-WSHP system model, the influences of four operating conditions on system energy efficiency were studied. The parameters for the standard group and the control group are listed in Table 2.

Table 2 Standard group and control group for the parametric analysis of DX-WSHP

Parameter	Unit	Standard group	Control group*
Gas cooler inlet pressure $P_{f,gc,in}$	MPa	10	7.5~12. interval 0.5
Superheat temperature T_{sh}	℃	4	2~6. interval 0.5
Evaporator (water side) inlet temperature $T_{w,evp,in}$	℃	12	8~16. interval 1
Evaporator (water side) flow rate $V_{w,evp}$	m^3/h	2	0.25. 0.5. 1. 3. 4

* Note: if the standard group values are included, they will be automatically deleted.

Based on the calculation result for the standard group, the COP of DX-WSHP is 3.38, which is improved by 31.0% compared to the 2.58 in research **Error! Reference source not found.**. This demonstrates that the DX-WSHP has excellent heat transfer and energy efficiency capabilities.

3.2.1 Influence of gas cooler inlet pressure and superheat temperature

Fig. 12 (a) shows the variation of COP and cooling capacity Q with respect to $P_{f,gc,in}$. When the $P_{f,gc,in}$ is greater than 8 MPa, with the increase in $P_{f,gc,in}$, the COP continuously decreases, while the Q slowly increases. However, when the $P_{f,gc,in}$ is reduced from 8 MPa to 7.5 MPa, both the COP and Q show a significant decrease. The decrease in Q is attributed to the fact that at this point, the gas cooler operation is approaching the critical point, which may lead to heat transfer deterioration and subsequently reduce the system efficiency.

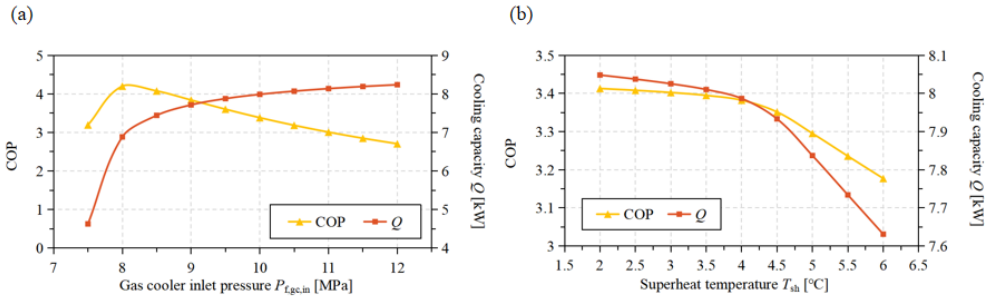

Fig.12 (a) Influence of gas cooler inlet pressure; (b) influence of superheat temperature

Fig. 12 (b) shows the variation of COP and Q with respect to T_{sh}. Both COP and Q decrease with the increase in T_{sh}, and the rate of decrease becomes more significant when the T_{sh} exceeds 4°C. However, the changes are not substantial, and compared to the standard group, the variations in COP and Q are within ±7%.

3.2.2 Influence of inlet temperature and flow rate of evaporator (water side)

Fig. 13 (a) shows the variation of COP and Q with respect to $T_{w,evp,in}$. Both COP and Q show a linear increase trend with the rise in the $T_{w,evp,in}$. However, the changes are not substantial, and compared to the standard group, the variation in COP is within ±15%, and the variation in Q is within ±10%.

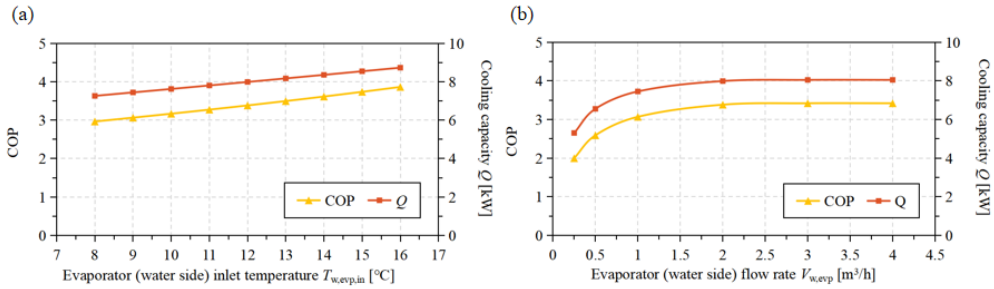

Fig.13 (a) Influence of evaporator (water side) inlet temperature; (b) influence of evaporator (water side) flow rate

Fig. 13 (b) shows the variation of COP and Q with respect to $V_{w,evp}$. Both COP and Q increase with the rise in the $V_{w,evp}$. However, when the $V_{w,evp}$ exceeds 2 m^3/h, both COP and Q have reached a relatively stable level.

4. Conclusions

In this paper, a direct-expansion wastewater source heat pump (DX-WSHP) is proposed, and a three-dimensional transient heat transfer model based on the thermal resistance and capacity model was established for a direct-expansion wastewater source heat exchanger (DX-WSHE). The model was then used to study the heat transfer characteristics under various parameter influences. Subsequently, a system model was developed to calculate the system's energy efficiency under different operating conditions. The following conclusions are drawn:

(1) With the decrease of CO_2 inlet pressure, the pressure drop of the system decreases, while with the increase of CO_2 inlet temperature, the heat exchange capacity per meter and pressure drop

increase linearly. With the increase of CO_2 mass flow, the heat exchange capacity increases synchronously, but the increasing range gradually decreases, and the pressure drop increases synchronously and the increasing range gradually increases.

(2) With the increase of sewage inlet temperature, the length of heat exchanger and the decrease of the outer diameter of heat exchange tube, the heat exchange capacity per linear meter decreases linearly and the pressure drop increases linearly. When the outer diameter of the sewage pipe is large, more heat exchange tubes can be added in the sewage pipe to increase the total heat exchange capacity. Different heat exchange tube materials have little influence on the direct expansion sewage source heat exchanger.

(3) When the inlet pressure of the air cooler is greater than 8 MPa, with the increase of the inlet pressure of the air cooler, the COP decreases continuously, while the cooling capacity increases slowly. However, when the inlet pressure of the air cooler dropped from 8MPa to 7.5 MPa, the COP and cooling capacity decreased significantly.

(4) With the increase of the inlet temperature and flow rate of circulating water in the evaporator, COP and cooling capacity increase linearly, but the change fluctuates little. When the circulating water flow rate is higher than 2 m^3/h, it basically tends to be stable. Both COP and cooling capacity decrease with the increase of superheat, and the decline rate is even greater when superheat is greater than 4℃.

(5) The coefficient of performance (COP) of the DX-WSHP can be increased by 31.0% compared to conventional design, and the heat flux of the DX-WSHE can be up to 250 W/m for the standard group.

(6) The DX-WSHP has excellent heat transfer and energy efficiency capabilities, and its long-term operational characteristics will be studied by integrating actual building load data and wastewater data.

Acknowledgment

This work was supported by National Natural Science Foundation of China (No.52306266), Science and Technology Program of China Huadian Corporation (No.CHDKJ22-01-23) and China Postdoctoral Science Foundation (No.2022M712347).

Nomenclature

Nomenclature

Symbols	
A	cross-sectional area (m^2)
d	diameter (m)
f	friction factor
h	convective heat transfer coefficient
m	mass flow rate ($kg \cdot s^{-1}$)
Pr	Prandtl number
Q	heat exchanged (W)
Re	Reynolds number
R	thermal resistance ($m \cdot K \cdot W^{-1}$)

T	temperature (°C)
u	velocity ($m \cdot s^{-1}$)
λ	thermal conductivity ($W \cdot m^{-1} \cdot K^{-1}$)
$\overline{\lambda}$	average thermal conductivity ($W \cdot m^{-1} \cdot K^{-1}$)
ρ	density ($kg \cdot m^{-3}$)
μ	dynamic viscosity (Pa·s)
$\overline{c}$	average specific heat capacity ($J \cdot kg^{-1} \cdot K^{-1}$)
τ	time (s)
η	efficiency
ΔL	Length (m)
ΔP	pressure drop (MPa)

Subscripts

c	waste water pipeline
f	CO_2
hyd	hydraulic diameter
inn	inner diameter
in, out	inlet, outlet
o	outer diameter
p	CO_2 pipeline
s	soil
w	waste water

References

References

[1] Mladen Bošnjaković, *et al.*, BUILDING INTEGRATED PHOTOVOLTAICS. OVERVIEW OF BARRIERS AND OPPORTUNITIES, *Thermal Science*, 27(2023), 2B, pp. 1433-1451

[2] Fang Xiaomin, Li Xiaolu, SOLAR PHOTOVOLTAIC POWER STATION SYSTEM BASED ON COMPOSITE HEAT SOURCE THERMAL POWER TECHNOLOGY, *Thermal Science*, 27(2023), 2A, pp. 967-973

[3] Xu Tongyu, *et al.*, Integration of sewage source heat pump and micro-cogeneration system based on domestic hot water demand characteristics: A feasibility study and economic analysis, *Process Safety and Environmental Protection*, 179(2023), pp. 796-811

[4] Shen Chao, *et al.*, A review on the current research and application of wastewater source heat pumps in China, *Thermal Science and Engineering Progress*, 6(2018), pp. 140-156

[5] Du Yuji, *et al.*, The potential of wastewater-source heat pump in decarbonizing buildings sector of China, *Environmental technology*, 2023, pp. 31-30

[6] Ozcan Huseyin Gunhan, *et al*., Energy, exergy, economic, environmental and sustainability (4ES) analyses of a wastewater source heat pump system for district heating applications based on real operational data, *Sustainable Energy Technologies and Assessments*, 56(2023), pp. 103077

[7] Wang Qiang, *et al*., Experiments on the characteristics of a sewage water source heat pump system for heat recovery from bath waste, *Applied Thermal Engineering*, 204(2022), pp. 117956

[8] Zhang Qunli, *et al*., Experimental evaluation of heat transfer performance of falling film evaporator for wastewater source heat pump with backwash system, *International Journal of Refrigeration*, 113(2020), pp. 80-93

[9] Liu Y, *et al*., VERTICAL U-SHAPED HEAT EXCHANGERS FOR CONSTRUCTION ENGINEERING: NEW PROMISES AND FUTURE CHALLENGES, *Thermal Science*, 25(2021), 3B, pp. 2253-2261

[10] Jokić I A, *et al*., FEASIBILITY OF CLOSED LOOP GROUND SOURCE HEAT PUMP FOR RESIDENTIAL HEATING AND COOLING APPLICATIONS IN SERBIA, *Thermal Science*, 24(2020), 2A, pp. 96-976

[11] Gao Yuefen, Gao Tingting, Simulation study on the performance of direct expansion geothermal refrigeration system using carbon dioxide transcritical cycle, in: *Energy Procedia*, Elsevier Ltd, Hong Kong, 2019, pp. 5479-5487

[12] A. Nguyen, *et al*., Pressure–enthalpy coupled thermal resistance and capacity model (PH-TRCM) for direct-expansion borehole heat exchangers: Application for supercritical CO_2, *Geothermics*, 76(2018), pp. 50-59

[13] Ghazizade-Ahsaee H, Ameri M, Energy and Exergy Investigation of a Carbon Dioxide Direct-Expansion Geothermal Heat Pump, *Applied Thermal Engineering*, 129(2018), pp. 165-178

[14] Ghazizade-Ahsaee H, Ameri M, Effects of using expander and internal heat exchanger on carbon dioxide direct-expansion geothermal heat pump, *Applied Thermal Engineering*, 136(2018), pp. 389-407

[15] Ghazizade-Ahsaee H, *et al*., A comparative exergo-economic analysis of four configurations of carbon dioxide direct-expansion geothermal heat pump, *Applied Thermal Engineering*, 163(2019), C, pp. 114347

[16] Lemmon E W, *et al*., NIST Standard Reference Database 23: Reference Fluid Thermodynamic and Transport Properties-REFPROP, in: *National Institute of Standards and Technology*, Standard Reference Data Program, Gaithersburg, 2013

[17] Eslami-Nejad P, *et al*., A quasi-transient model of a transcritical carbon dioxide direct-expansion ground source heat pump for space and water heating, *Applied Thermal Engineering*, 91(2015), pp. 259-269

[18] Li Y, *et al*., Dynamic heat transfer analysis of a direct-expansion CO_2 downhole heat exchanger, *Applied Thermal Engineering*, 189(2021), pp. 116733

[19] Austin B T, Sumathy K, Parametric study on the performance of a direct-expansion geothermal heat pump using carbon dioxide, *Applied Thermal Engineering*, 31(2011), 17, pp. 3774-3782

Submitted: 23.12.2023

Revised: 19.02.2024

Accepted: 14.03.2024